D S 21, 2006
Preprint typeset using LaTeX style emulateapj v. 11/27/05

ON RELAXATION PROCESSES IN COLLISIONLESS MERGERS

M V ,[1,2] I M. V ,[3,2] S K ,[1,2] A V. K [1,2,4] C L.B [5]

Draft version September 21, 2006

ABSTRACT

We analyze *N*-body simulations of halo mergers to investigate the mechanisms responsible for driving mixing in phase-space and the evolution to dynamical equilibrium. We focus on mixing in energy and angular momentum and show that mixing occurs in step-like fashion following pericenter passages of the halos. This makes mixing during a merger unlike other well known mixing processes such as phase mixing and chaotic mixing whose rates scale with local dynamical time. We conclude that the mixing process that drives the system to equilibrium is primarily a response to energy and angular momentum redistribution that occurs due to impulsive tidal shocking and dynamical friction rather than a result of chaotic mixing in a changing potential. We also analyze the merger remnants to determine the degree of mixing at various radii by monitoring changes in radius, energy and angular momentum of particles. We confirm previous findings that show that the majority of particles retain strong memory of their original kinetic energies and angular momenta but do experience changes in their potential energies owing to the tidal shocks they experience during pericenter passages. Finally, we show that a significant fraction of mass ($\approx 40\%$) in the merger remnant lies outside its formal virial radius and that this matter is ejected roughly uniformly from all radii outside the inner regions. This highlights the fact that mass, in its standard virial definition, is not additive in mergers. We discuss the implications of these results for our understanding of relaxation in collisionless dynamical systems.

Subject headings: cosmology: theory — dark matter:halos — galaxies: relaxation — halos: structure — methods: numerical

1. INTRODUCTION

Almost four decades have passed since "violent relaxation" was first proposed by Lynden-Bell (1967) as a mechanism to explain the remarkable regularity and smoothness of the light distributions in elliptical galaxies. Several authors had noted that the time scale for two-body relaxation (Chandrasekhar 1943) was several orders of magnitude too long to be relevant for the evolution of galaxies (Zwicky 1939). Lynden-Bell derived the distribution function that would result from rapid fluctuations in the potential of the galaxy, such as those that might occur during gravitational collapse or following a merger. The process of violent relaxation outlined by Lynden-Bell produces a smooth distribution function as a result of the gravitational scattering of particles by the time dependent global gravitational potential. He argued that this process could result in a mass-independent and smooth final distribution of particles in phase-space.

Another process that was considered by Lynden-Bell (1967) is "phase mixing" - a process by which an initially compact ensemble of non-interacting phase-space points in a time-independent potential can be stretched into a long ribbon in phase-space as a result of small differences in the initial energies (or angular momenta) of particles in the ensemble. Phase mixing conserves the fine grained distribution function but in a coarse grained sense it produces smooth/relaxed looking distributions on timescales that depend only on the range of values of the orbital integrals (or actions) in the ensemble (Binney & Tremaine 1987).

[1] Department of Astronomy and Astrophysics, University of Chicago, 5640 S. Ellis Avenue, Chicago, IL 60637
valluri@kicp.uchicago.edu
[2] Kavli Institute for Cosmological Physics, The University of Chicago, Chicago, IL 60637
[3] Department of Astronomy, University of Florida, Gainesville, FL 32611
[4] Enrico Fermi Institute, The University of Chicago, Chicago, IL 60637
[5] Department of Physics, Northern Illinois University, DeKalb, IL 60115

In the last decade, a new type of mixing process, which occurs due to the presence of large fractions of chaotic orbits in a galactic potential (such as when box orbits are scattered by a central supermassive black hole in a triaxial galaxy), has been investigated (Mahon et al. 1995; Merritt & Valluri 1996; Habib et al. 1997; Kandrup et al. 2000; Kandrup & Siopis 2003). These studies have shown that microscopic ensembles of iso-energetic test particles which occupy an infinitesimal volume of phase-space surrounding a chaotic orbit can evolve rapidly to a near-invariant distribution that uniformly covers the energy surface available to the ensemble. This process of diffusion to a near-invariant distribution is termed "chaotic mixing" and has been shown to occur in a variety of galaxy-type potentials. These authors argued that in a triaxial galaxy with a supermassive central black hole, a significant fraction of orbits are chaotic, and consequently, this mixing process could drive secular evolution to more axially symmetric distributions.

The physically interesting aspect of this mixing process is that the evolution to a near-invariant distribution has been shown to occur on timescales of order 5 to 100 orbital crossing times in strongly chaotic systems making it a potentially important process for the evolution of galaxies. This was demonstrated by Merritt & Quinlan (1998) who employed *N*-body simulations of triaxial elliptical galaxies containing growing supermassive central black holes and found the triaxial figures to evolve to more axisymmetric shapes.

Like phase mixing, chaotic mixing conserves the fine-grained phase-space density. Unlike phase mixing, its rate does not depend on the initial spread in the energy distribution of particles in the ensemble, but on how strongly chaotic the orbits in the ensemble are (Merritt & Valluri 1996).

However two concerns remain regarding these earlier experiments. First the rate of evolution to the invariant measure depends on the properties of the ensemble of particles. For ensembles near a "sticky" or weakly chaotic orbit, a near-

invariant distribution may not be attained in the lifetime of the galaxy (Merritt & Valluri 1996). Second, the majority of the numerical studies which found strong chaotic mixing and short time scales for evolution were not carried out in self-consistent potentials leading to concerns that in self-consistent systems such mixing could be self-limiting.

Since all orbits in a time-dependent potential with long-lived oscillations can, in principle, exchange energy with the potential, a large fraction of the orbits will not conserve the energy integral. In such systems previous authors have found that a significant fraction of orbits can be chaotic (Kandrup et al. 2003). This raises the possibility that the underlying physical process driving relaxation in violently fluctuating potentials could be a consequence of chaotic mixing. The first step in making this connection was studied by Kandrup et al. (2003) and Terzić & Kandrup (2004), who demonstrated that large fractions of chaotic orbits arise in potentials subjected to long-duration (damped) periodic oscillations. These authors found that the fraction of chaotic orbits depended on the frequency as well as the amplitude of the oscillations in the potential and attributed the chaos to a "broad parametric resonance".

In this paper we analyze the mechanisms driving the approach to equilibrium following the collisionless merger of two self-gravitating systems. Our principal interest is in understanding whether changes in the fine-grained distribution function (e.g., changes in the angular momenta and energies of nearby particles) occur as a result of exponential instabilities of orbits or some more straightforward energy exchange process which transfers kinetic energy of the merging halos to the internal energies of particles.

We consider two dynamical heating effects that are not usually discussed in this context. The first is the effect of compressive tides that arise when one collisionless gravitating system passes through another on a time scale that is short compared to the internal dynamical time of the infalling system. Such tides can impulsively heat particles as a result of the transient deepening of the net potential. Impulsive compressive tidal shocks have been studied previously and are well known to produce large changes in the internal structure and evolution of globular clusters (Spitzer & Chevalier 1973; Gnedin et al. 1999), galaxies orbiting within a cluster potential (Valluri 1993), and DM subhalos orbiting within larger hosts (Kravtsov et al. 2004; Kazantzidis et al. 2004b).

The second process is dynamical friction (Chandrasekhar 1943), which is the primary mechanism that causes the formation of a single remnant when two collisionless halos merge. When collisionless halos merge, dynamical friction transfers their relative linear and angular orbital momenta to the individual particles. The original version of the Chandrasekhar (1943) dynamical friction theory applied to the deceleration of a massive star moving in an infinite homogenous isotropic stellar distribution. However several studies have shown that with minor modifications the theory is applicable in systems that resemble real galaxies and clusters (White 1976; Binney 1977; Velazquez & White 1999). Dynamical friction is found to be enhanced in systems with inhomogenous density profiles (such as cuspy profiles Del Popolo 2003), as compared with systems with uniform homogenous distributions. Recent N-body studies of live satellites in extended N-body galaxies (Jiang & Binney 2000; Fujii et al. 2006) have shown that the timescale for dynamical friction is shorter than that predicted by Chandrasekhar due to two additional components of drag force: the tidal torque from the leading tidal tail and an enhanced wake due to particles that are no longer bound to the satellite but still trail behind it in the same orbit.

It is important to emphasize at the outset, that the terms "mixing" and "relaxation" are often used rather loosely (and often interchangeably) in the astrophysics literature to mean the approach of a gravitating system to global as well as small-scale equilibrium. The most restrictive definition of "relaxation" is a process which leads to the complete "loss of memory of initial conditions" or loss of correlations between initially nearby particles in phase space. The large changes in integrals of motion required for such relaxation only occur as a result of two-body interactions (Chandrasekhar 1943) and as a result of "violent relaxation". Both processes cause changes in the fine-grained distribution function. In contrast phase mixing and chaotic mixing in time-independent potentials, under the right conditions, can lead to large changes in correlations but conserve integrals of motions (if they exist) and conserve the fine-grained distribution function. In this paper we focus our attention on loss of correlations in phase space accompanying a collisionless merger and use the term "mixing" to connote the approach to macroscopic equilibrium and the accompanying change in the fine-grained distribution function (even though this is quite small).

According to the prevailing cosmological model for structure formation, galaxies and dark matter (DM) halos in the Universe form hierarchically via multiple mergers. Numerous minor mergers and several major mergers of subhalos eventually form the dark halos at $z = 0$. Thus, the merger history of cosmological structures is complex, and DM halos are predicted to abound in substructure and have mass profiles that may still be evolving today. A detailed analysis of the physics of gravitational relaxation, with the specific goal of understanding what processes drive the DM and stellar component to equilibrium, can be more readily done using dissipationless controlled merger simulations.

The discovery of universal dark matter halo profiles resulting from cosmological N-body simulations (e.g., Dubinski & Carlberg 1991; Navarro et al. 1996, 1997; Merritt et al. 2005; Graham et al. 2005), and the more recent finding that phase-space density profiles of these halos have power-law distributions (Taylor & Navarro 2001; Arad et al. 2004; Ascasibar & Binney 2005) has led to a resurgence in interest in the processes that cause relaxation in self-gravitating systems. In particular, violent relaxation and the statistical distribution functions that result from this process are being actively investigated (Arad & Lynden-Bell 2005; Arad & Johansson 2005; Dehnen 2005). Several studies of the remnant density profiles have shown that the remnants retain a surprisingly strong memory of their initial density profiles despite the strength of the relaxation process (Boylan-Kolchin & Ma 2004a; Kazantzidis et al. 2006).

Several authors have criticized Lynden-Bell's 1967 original suggestion that it is potential fluctuations that occur during gravitational collapse that drive the system to equilibrium, on the grounds that time dependence of the potential alone merely causes particles to be relabeled in energy and causes no mixing of nearby particles in energy and angular momentum. It has been therefore argued that a process like chaotic mixing is actually responsible (at the microscopic level) for driving the evolution of the system to equilibrium (Merritt & Valluri 1996; Kandrup et al. 2003).

An analysis of the merging process can help us better understand the physical mechanisms that drive the evolution to equilibrium and cause the redistribution of nearby particles

in phase-space. In this investigation we restrict ourselves to the study of mixing in positions, velocities, energies and angular momenta of particles. The goals of this study are: (a) to determine whether the relaxation of a remnant to an equilibrium distribution following a collisionless N-body merger is driven by chaotic mixing that is believed to take place in time-independent potentials (b) to quantify the degree of relaxation/mixing in various phase-space parameters that occurs during the merger by examining the remnants of major mergers of DM halos, and (c) to obtain a better understanding of why steep cusps are as robust as they are. Both the time-dependent nature of the problem, as well as the fact that N-body systems exhibit exponential sensitivity to initial conditions (as discussed in greater detail in § 2.2), make the first of the above goals particularly challenging.

The paper is organized as follows. In § 2 we describe the N-body experiments that were conducted and define several new measures that we use to quantify the rate of separation of nearby orbits and the degree of "mixing" or "relaxation" in phase-space. In § 3 we discuss the results of the application of our measures of mixing to the merger experiments by considering the separation in various phase-space variables of pairs of nearest neighbors in phase-space (§ 3.1) as well as by monitoring the rate of mixing of ensembles of nearby particles (§ 3.2). In § 4 we examine how particles are redistributed in phase-space following the merger. In § 5 we summarize our results and discuss the implications of our findings for understanding relaxation during mergers and the mixing that it produces.

2. NUMERICAL METHODS

We investigate the mechanisms responsible for violent relaxation by analyzing N-body simulations of binary mergers between dark matter halos. The halo models follow density profiles that are described by the general (α,β,γ) spherical density law (e.g., Zhao 1996), where γ denotes the asymptotic inner slope of the profile, β corresponds to the outer slope, and α is the transition slope between the inner and outer profiles.

We consider two main halo models specified by particular choices of the parameters α, β, and γ. The first model follows the Navarro et al. (1996, hereafter NFW) profile (with $(\alpha,\beta,\gamma) = (1,3,1)$), while the second model (with $(\alpha,\beta,\gamma) = (2,3,0.2)$) corresponds to a profile with a shallower inner slope. N-body halo models are constructed using the exact phase-space distribution function under the assumptions of spherical symmetry and an isotropic velocity dispersion tensor (Kazantzidis et al. 2004a). Each of the initial DM halos has a virial mass of $M_{\rm vir} = 10^{12} M_{\odot}$ implying a virial radius of $r_{\rm vir} \simeq 256.7$ kpc, and a concentration of $c = 12$, resulting in a scale radius of $r_{\rm s} \simeq 21.4$ kpc. It is worth emphasizing that the adopted value of $M_{\rm vir}$ serves merely practical purposes and does not imply anything special about the particular choice of mass scale. Hence, our conclusions can be readily extended to mergers between equal-mass systems of any mass scale.

We analyze three different merger experiments which were conducted with the multi-stepping, parallel, tree N-body code PKDGRAV (Stadel 2001). PKDGRAV uses a spline softening length, such that the force is completely Keplerian at twice the quoted softening length, and multi-stepping based on the local acceleration of particles. The first experiment followed the encounter of two NFW halos (referred to hereafter as run Bp1), while in the second experiment an NFW halo merged with a halo having an inner slope of $\gamma = 0.2$ (referred to hereafter as run hBp1). The initial halo models in these two runs were sampled with $N = 2 \times 10^5$ particles and forces were softened with a spline gravitational softening length equal to $\epsilon = 1.5$ kpc. In order to minimize any concern that our results might be compromised by numerical resolution effects, we analyzed an additional merger experiment between two NFW halos increasing the mass resolution by a factor of 10 and scaling down the softening lengths according to $\epsilon \propto N^{-1/3}$ (hereafter referred to as run HRBp). Initial conditions for binary mergers were generated by building pairs of halo models and placing them at a distance equal to twice their virial radii. In this study we only discuss mergers of systems on parabolic orbits owing to the fact that this particular orbital configuration is the most typical of merging halos in cosmological simulations (e.g., Zentner et al. 2005). These merger simulations (labeled Bp1,hBp1, and HRBp) were described in greater detail in Kazantzidis et al. (2006).

In order to distinguish the mixing that results from the exponential instability of the N-body problem (see § 2.2) from the effects of the mixing resulting during the merger, we also performed N-body simulations of the evolution of a spherical isolated NFW halo. All orbits in an isolated spherical halo are expected (in the smooth potential or large N limit) to be "regular orbits" that conserve four isolating integrals of motion. This simulation therefore serves as an important control experiment with which to compare the evolution in the merger simulations.

2.1. *Macroscopic Evolution of Merger Remnants*

A self-gravitating distribution of particles that is out of equilibrium will experience potential fluctuations, and the potential and kinetic energies of particles will oscillate back and forth. This behavior is governed by the time-dependent virial theorem:

$$\frac{1}{2}\ddot{I} = 2T + V \tag{1}$$

where I is the moment of inertia, T is the total kinetic energy, and V is the total potential energy of the system of particles, with all quantities defined with respect to the center of mass of the system. For a time-independent gravitating system, $\ddot{I} = 0 = 2T + V$. A robust quantitative measure of how far a gravitating system is from equilibrium can be obtained from the virial ratio $2T/|V|$, which is unity for a system in global dynamical equilibrium.

In Figure 1, the top panel shows the separation of the most-bound-particle (MBP) of each halo in the merger and the lower panel shows the evolution of the virial ratio $2T/|V|$, as a function of time. We note that pericenter passages (seen as minima in the MBP separation) correspond to maxima in the virial ratio and vice versa. For $t \lesssim 7$ Gyr the virial ratio $2T/|V|$ undergoes strong fluctuations and remains close to unity thereafter. We refer to this time $t \sim 7$ Gyr to be the time when the system is *globally relaxed*.

2.2. *Microscopic Chaos or the Miller Instability*

In real galaxies, there are two components of the gravitational accelerations on particles, a component arising from the background potential which is smoothly varying with time, and a second component arising from the discrete nature of stars (and possibly dark-matter particles). The importance of the discrete component is defined by the two-body relaxation timescale (Chandrasekhar 1943; Binney & Tremaine 1987) and is larger than the age of the Universe in galaxy-sized systems. Therefore, it is generally assumed that equilibrium and

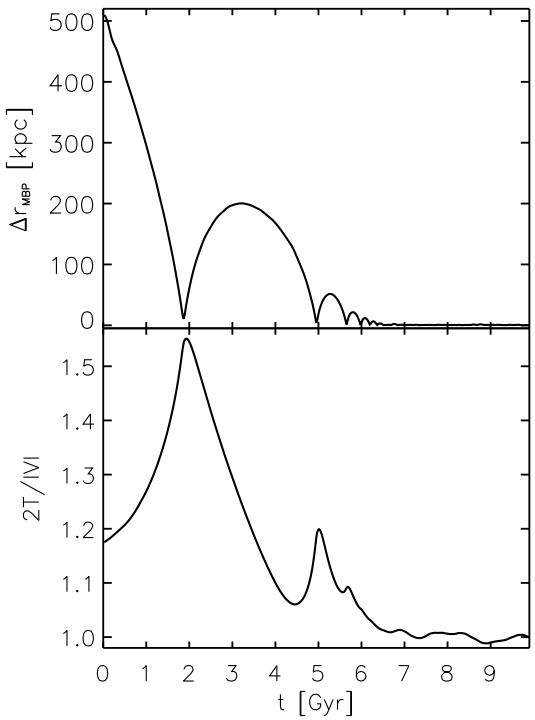

F . 1.— Top: The separation between the most-bound particles of the two merging NFW halos (run Bp1) as a function of time; Bottom: time evolution of the virial ratio $2T/|V|$.

non-equilibrium evolution of the phase-space density distributions in galaxy-size objects can be studied in the mean-field limit, where the collisionless Boltzmann equation can be applied.

The Lyapunov exponent (Lichtenberg & Lieberman 1992) is one of the most popular ways of measuring the chaoticity of an orbit in a smooth potential. It measures the rate of divergence of two infinitesimally nearby orbits in phase-space. If the rate of divergence of phase-space points is linear, then the Lyapunov exponent $\lambda = 0$ and the orbit is termed *regular*. In a smooth equilibrium potential with three-spatial dimensions such orbits will conserve at least three isolating integrals of motion. If, on the other hand, the rate of divergence of the phase-space points is exponential, the orbit is termed *chaotic*. Thus, the Lyapunov exponent defines the time scale on which infinitesimally nearby trajectories in phase-space undergo exponential separations in their phase-space coordinates.

However, as was first noted by Miller (1964), the N-body problem is chaotic in the sense that the trajectory of the $6N$-dimensional phase-space coordinate of the system exhibits exponential sensitivity toward small changes in initial conditions. This exponential instability (referred to in the literature as the "Miller instability"; e.g., Hemsendorf & Merritt 2002 or "microchaos" Sideris & Kandrup 2002) has been investigated extensively in several studies over the past three decades (see Merritt 2005 for a review). These studies have shown that the largest N-body Lyapunov exponent λ does not converge toward zero as N increases (Kandrup & Smith 1991a; Goodman et al. 1993), even for N-body realizations of integrable potentials (Kandrup & Sideris 2001).

In fact more recently Hemsendorf & Merritt (2002) have shown that the direct N-body problem (with $N < 10^5$) is inherently chaotic and that the degree of chaos, as measured by the rate of divergence of nearby trajectories (with the Lyapunov exponent λ), increases with increasing N with characteristic e-folding time equal to $\sim 1/20$ of the system crossing time. It has also been shown that the mean t_e (e-folding time) increases as the softening parameter is increased so that discreteness effects are reduced as the softening becomes comparable to interparticle separations (Kandrup & Smith 1991b).

The exponential separation of particles in energy occurs on the Miller instability timescale (t_e) which is much smaller than the two body relaxation time (t_r) (Kandrup et al. 1994; Hut & Heggie 2001). The divergence of particles in energy saturates after a few t_e and then varies with time on the standard two-body relaxation timescale indicating that the Miller instability is not an important process in changing the fine-grained distribution functions of gravitating systems.

Despite the fact that particles separate exponentially in phase space, as N increases orbits in these systems become more and more regular, acquiring orbital characteristics closer and closer to those in smooth potentials, and the macroscopic separations of orbits saturate at smaller and smaller distances (Valluri & Merritt 2000; Kandrup & Sideris 2001; Sideris 2004). Additionally, decades of N-body integrations have demonstrated that, in many ways, the behavior of large-N systems matches expectations derived from the collisionless Boltzmann equation (e.g., Aarseth & Lecar 1975).

The fact that in an N-body system the Lyapunov exponent will primarily measure the "Miller instability" and not macroscopic chaos (arising from the background potential) means that it is has limited usefulness for measuring chaotic behavior in N-body systems. Other measures of chaos, such as those that measure changes in orbital characteristics (for instance, fundamental oscillation frequencies of orbits; e.g., Laskar 1990, Laskar et al. 1992, Valluri & Merritt 1998), rely on the ability to identify such frequencies from oscillations that last between 30-100 orbital periods. Recently, a new technique based on pattern recognition of orbital characteristics has been developed and is applicable in time-dependent systems whose oscillations last 10-30 crossing times (Sideris 2006). To our knowledge, none of the standard measures of chaos are applicable to N-body orbits in potentials with non-periodic potential fluctuations lasting only a few (< 10) crossing times. This makes it necessary to define new ways of quantifying chaos and mixing.

2.3. *Definition of mixing in N-body systems*

In this paper we estimate the degree of mixing at various stages of the evolution of the merging systems (a) by considering *pairs* of nearby particles in the N-body simulation and tracing their separation in four different phase-space quantities and (b) by carrying out *mixing experiments* that monitor the rate at which *ensembles* of 1000s of nearby particles evolve with time and reach a "near invariant" distribution in energy and angular momentum.

2.3.1. *Separation of pairs of nearby particles*

Several previous studies of this type have focused on the configuration space separation Δr of a pair of infinitesimally nearby test particles in a frozen N-body potential. These studies picked pairs of non-self-gravitating test particles that are arbitrarily nearby in phase-space (Valluri & Merritt 2000; Kandrup & Sideris 2003). Studies that used live N-body simulations (e.g., Kandrup et al. 1994) have compared pairs of orbits in two different realizations of simulations where the initial conditions had been perturbed by an infinitesimal amount.

Here we work with orbits in a given N-body simulation and are therefore limited (by the resolution of the simulations) in our ability to choose pairs of particles that are very close in phase-space.

We select a large number (1000) of nearest-neighbor pairs in one of the two merging N-body halos and follow their separations through the entire merger process. We have checked that when two identical halos merge, the results were independent of the halo chosen to perform the analysis. To pick particle pairs we adopt the following scheme:

1. All the particles in a given halo are sorted in their separation r from the MBP of that halo, and the particles are binned in ten radial shells of equal width, extending from the MBP to the initial virial radius of the halo ($r_{\rm vir} \simeq 256.7$ kpc). In the analysis that follows we compare behavior of particles in the 1st, 4th and 7th shell from the center of the potential. The outer radius of the first shell is just outside the scale radius, the 4th shell lies at the half mass radius and 7th shell lies at the 3/4 mass radius of the initial NFW halo.

2. A particle P^* with separation $r_{\rm P}$ from the MBP is picked at random in a given shell, and the 5000 nearest particles in configuration space to the particle P^* are selected.

3. The velocity separations $|v|$ of each of the 5000 particles relative to particle P^* are computed, and the 2500 particles with the smallest $|v|$ separation from P^* are selected.

4. The magnitudes of the separation of total angular momentum J of each of the 2500 particles above relative to particle P^* are computed, and the 1250 particles with the smallest J separation from P^* are selected.

5. The angle between the angular momentum $\mathbf{J}$ and the angular momentum $\mathbf{J}_{P^*}$ is computed for each of the 1250 particles, and the 625 particles with the smallest angle are selected.

6. From the remaining 625 particles, the particle with the total energy $E = T + V$ closest to the particle P^* is then picked as its nearest neighbor.

In general, after an initial phase of exponential growth, the separation of two nearby particles saturates and then oscillates about some median value, due to small but finite differences in the initial oscillation frequencies in the global potential (e.g., Kandrup & Sideris 2003). To determine the behavior of a "typical pair" of particles in a given shell, we first pick 1000 pairs of particles in each shell. We then report the median value of the separation of that phase-space quantity as a function of time for the 1000 particle pairs. We find (as is well known) that the median is a more reliable estimator than the mean separation of particles because each particle has a small but finite probability of being ejected from the system as a result of the merger, and such ejections cause a small fraction of particles to form a long tail in the histogram of separations at each time step. Thus, for all quantities defined below it should be implicitly understood that we report the median value of the parameter for 1000 pairs of particles. Specifically, we monitor the following quantities.

1. "$\ln(\Delta r)$" – the natural logarithm of the separation in the spatial coordinate r of the median pair of particles.

2. "$\ln(|\Delta v|)$" – the natural logarithm of the absolute value of the relative three dimensional velocity v of the median pair of particles.

3. "ΔE" – the separation in total energy of the median pair of particles.

4. "ΔJ" – the separation in the total amplitude of the angular momentum of the median pair of particles. (We pick pairs whose vector directions have angular separations of less than 90 deg. As the particles separate, we track the separation in the amplitude of $\mathbf{J}$ but not the direction.)

The quantities defined above differ in one important aspect from previous studies in which similar quantities have been used: all particles in the pairs are self-gravitating (and not test particles) and are picked from an initial distribution function that is self-consistent with the spherical NFW potential. This implies that the typical initial pair separation $\ln(\Delta r)$ of particles depends on their location in the potential such that pairs in the central cusp will be much closer than the typical initial pair separation in the outer regions. We therefore often scale the quantities relative to their values at $t = 0$ Gyr. Moreover, especially when calculating the velocity separation $\ln(\Delta v)$, we observe the mutual gravitational attraction of nearby particles.

The quantities ΔE and ΔJ provide additional insights because in the case of an isolated N-body halo, both quantities are expected to remain constant (to within numerical errors) for the entire duration of the simulation (following the initial increase in these quantities due to the Miller instability). Since E and $\mathbf{J}$ are integrals of motion in equilibrium potentials, any changes in the separation of these quantities in the case of the merger reflects the influence of the time-dependent potential. Evolution with time of these quantities for various simulations are described in § 3.1.

2.3.2. *Mixing of ensembles in phase space*

Another way to quantify the mixing rate is by monitoring the secular evolution of ensembles of infinitesimally nearby test particles due to the presence of chaotic orbits. We conducted a series of mixing experiments where we monitored the spread of an ensemble of 1000 nearby particles as a function of time in two phase-space coordinates.

Such experiments have been carried out previously to study the mixing of microscopic ensembles of chaotic orbits in static, non-linear potentials (Mahon et al. 1995; Merritt & Valluri 1996; Kandrup et al. 2000; Kandrup & Siopis 2003). These authors picked ensembles of orbits with initial conditions that uniformly sampled an infinitesimally small region of phase-space and measured the rate at which the ensemble spreads and fills a region of configuration space. Ensembles associated with strongly chaotic orbits were found to evolve to a near-invariant distribution within 5-10 orbital crossing times, while ensembles associated with weakly chaotic or "sticky" orbits (orbits that lie close to resonance in phase-space) evolved on much longer time scales and often did not reach an invariant distribution. Ensembles associated with regular orbits only spread slightly, due to phase mixing that resulted from the small differences in their initial integrals of motion.

Once again the resolution of the simulations determine how closely we can sample the phase-space. We pick ensembles of the nearest 1000 particles about a given particle (P^*) in the

higher resolution merger simulation only (run HRBp), following a scheme similar to that for picking pairs of nearby particles (§ 2.3.1) to obtain the 1000 nearest particles to P^*.

Configuration-space coordinates have traditionally been used to study chaotic mixing of microscopic ensembles in smooth potentials. In such experiments microscopic ensembles of regular orbits do not mix at all in configuration space so all the observed mixing can be attributed to chaos. However tests carried out with ensembles selected by the above scheme in the N-body isolated spherical NFW halo showed quite significant spreading in configuration-space. The evolution of the ensembles in configuration space coordinates followed the following pattern: ensembles spread rapidly in configuration space on a short timescale (due to the Miller instability, see 2.2), and then continued to spread more slowly at a rate that scaled with local orbital period. At a given radius the mixing rate was found to be sensitive to the particular ensemble in question - the nature of the parent orbit (whether it is box-like or tube-like), the location of the orbit relative to the orientation of the merger etc. Since their mixing in configuration space is dominated by the Miller instability and phase mixing, our ensembles are too large to be usefully compared with the microscopic ensembles used to measure chaotic mixing in the works of previous authors. However, we found that ensembles selected by the above scheme in the isolated halo showed negligible mixing in the coordinates $E, \mathbf{J}$ (in agreement with the previous findings of Hut & Heggie 2001). Consequently we focus our attention on mixing in these two variables. The main objective of carrying out these experiments is to observe mixing in E, J that results from the merger.

We define the quantities $(\mathcal{E}, \mathcal{J})$ for each particle in the ensemble as follows:

$$\mathcal{E} = \frac{E - E(P^*)}{E(P^*)} \tag{2}$$

$$\mathcal{J} = \frac{J - J(P^*)}{J(P^*)} \tag{3}$$

where $E(P^*), J(P^*)$ are the energy, magnitude of the total angular momentum of the particle P^* respectively. The quantities $\mathcal{E}, \mathcal{J}$, are computed for each of the 1000 particles in the ensemble.

The results of these experiments are described in § 3.2.

3. RESULTS

3.1. *Separation of Nearby Particles in Phase-Space*

We begin by demonstrating the ability of the four quantities ($\ln(\Delta r)$, $\ln(\Delta|v|)$, ΔE and ΔJ) to identify mixing in phase space. All quantities are compared to equivalent quantities measured in an isolated equilibrium NFW halo to control for exponential instabilities due to the discrete nature of the simulations. Figure 2 shows the evolution of $\ln(\Delta r)$ and $\ln(\Delta v)$ as a function of time in 3 different radial shells (1st, 4th and 7th from the center). The quantities plotted are scaled using the initial values of the quantities at $t = 0$ Gyr; i.e., the top panels show $[\ln(\Delta r)/\ln(\Delta r(0))]$ and the lower panels show $[\ln(\Delta|v|)/\ln(\Delta|v(0)|)]$ (where $r(0), v(0)$ are the separations at $t = 0$). The solid lines show the evolution of the quantities in the low-resolution merger simulations (run Bp1: two NFW halos with 2×10^5 particles per halo), and the dot-dashed curves show the evolution of these quantities in the isolated equilibrium N-body NFW halo. In what follows we point out some characteristic features of this figure that are seen elsewhere in this section.

The top three panels of Figure 2 show that in both the merger and the isolated halo the initial separation is nearly linear in the quantity $\ln(\Delta r)$, indicating an exponential change in Δr. This constitutes a clear manifestation of the Miller instability (see § 2.2). This phase of exponential divergence is short lived (< 25% of the crossing time at a given radius). The e-folding time of the Miller instability (t_e) is shorter in the innermost shell (and is of order 1/20 the local crossing time in agreement with the findings of Hemsendorf & Merritt 2002) and increases with the radius of the shell. The increase of t_e with local crossing time is expected from previous studies of the Miller instability. In both the merger simulation and in the isolated halo, the initial rapid change in $\ln(\Delta r)$ saturates at the same value - a value determined by the length scale over which the smooth potential dominates over the graininess (Kandrup & Smith 1991b). At smaller radii, where the particle densities are higher, the saturation values are higher than at larger radii.

The lower panels of Figure 2 show the separation in $\ln(\Delta|v|)$ in both the isolated halo and the merging halos. There is a noticeable initial decrease in $\ln(\Delta|v|)$, which we attribute to the mutual gravitational attraction between the pair of particles that causes a deceleration of the particles while their radial separation increases. The initial decrease in $\ln(\Delta|v|)$ is seen in both the merging halos and the isolated halo, confirming that this is not due to the merger but is a characteristic of the N-body simulation.

In the innermost (1st) shell, after the initial growth in $\ln(\Delta r)$ and the initial decrease in $\ln(\Delta|v|)$, there are periods of time during which these quantities are essentially constant, separated by several sharp decreases in $\ln(\Delta r)$ and correspondingly sharp peaks in $\ln(\Delta|v|)$ not seen in the isolated halo. The dips in $\ln(\Delta r)$ and peaks in $\ln(\Delta|v|)$ are coincident with each other and correspond to the pericenter passages of the MBPs of the two halos seen in Figure 1. It is the first and second pericenter passages that cause the most significant changes in the particle separations ($\ln(\Delta r)$, $\ln(\Delta|v|)$).

It is quite remarkable how little systematic change in separation of either r or v is seen in between pericenter passages, suggesting that very little change in the macroscopic separations of particles occurring at any time during the merger except during the pericenter passages. This can be understood as follows: during pericenter passages of the centers of masses of the two halos, there is significant overlap in the two potentials leading to a sudden deepening in the potential experienced by the particles leading to a transient *compressive* tidal field that simultaneously decreases the separations in particles (seen by the dips in $\ln(\Delta r)$) and increases their kinetic energies (seen in the sharp increases in $\ln(\Delta|v|)$). Dynamical friction between the two halos is also strongest at pericenter and consequently the majority of their orbital energy and angular momentum are lost impulsively at these times. When the two halos separate enough that their innermost shells no longer overlap they experience little or no change in their potentials, so there is little further change in separation of trajectories. Thus, the global potential fluctuations that occur between pericenter passages do not cause any further increase in particle separations. Behavior similar to that in shell 1 is seen in shells 2 and 3 but is not shown here.

The effect of the first pericenter passage is seen to occur simultaneously at all radii. In shells 4, 7 we observe a dip in $\ln(\Delta r)$ and peak in $\ln(\Delta|v|)$ at the first pericenter passage which is both broader and less intense than in shell 1. At larger radii the first pericenter passage is followed by a con-

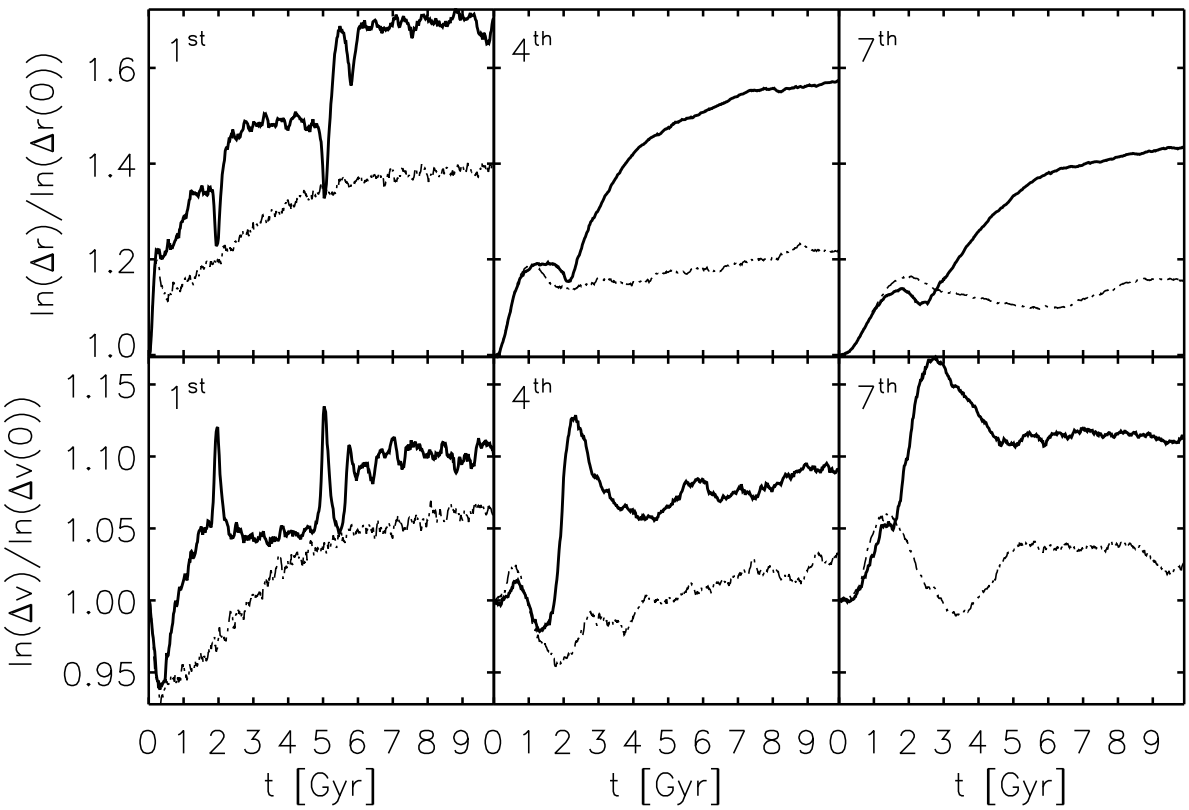

F . 2.— The top three panels show divergence in the quantities $\ln(\Delta r)/\ln(\Delta r(t=0))$ as a function of time for three different shells in the halo (from left to right: the first, fourth, and seventh shells respectively). The lower three panels show the quantity $\ln(\Delta|v|)/\ln(\Delta|v(t=0)|)$, for the same three shells. The solid lines are for the merger of two NFW halos (run Bp1). The dot-dashed lines are for the control simulation of an isolated NFW halo.

tinuous change in $\ln(\Delta r)$ and $\ln(\Delta|v|)$ but subsequent pericenter passages are less clearly visible. This indicates that while there is no propagation delay in the impulsive tidal shock with radius, the response is longer lived at larger radii. This is because, the centers of the two merging halos do not separate beyond the radius of the 4th and 7th shells after the first pericenter. Consequently the change in the external potential is not as sudden as for the inner shells.

As discussed in § 2.3 it is extremely difficult to make a reliable quantitative measurement of an exponential instability on a short timescale. However, both the qualitative and quantitative behavior of initially nearby particles seen in Figure 2 indicates that we are in fact detecting the Miller instability. If the oscillating external potential is also contributing to an exponential instability of orbits one might expect that if pairs of nearby particles were picked during the phase when the potential is changing very rapidly, the rate of separation in some quantity (say r) would be greater than in either the isolated halo or at the start of the merger. Figure 3 compares the separations of particles $\ln(\Delta r)$ when pairs were picked at $t = 0$ Gyr with pairs picked at $t = 0$ Gyr in the isolated halo and separation of pairs of particles picked at $t = 3$ Gyr. For the pairs of particles picked at $t = 3$ Gyr in the merger, the time axis is $t - 3$ so that initial slopes of the three curves can be more readily compared. We chose a start time $t = 3$ Gyr to compare against since it corresponds to a time at which the virial ratio is changing very rapidly and corresponds to the first apocenter separation of the MBPs of the two halos (identical behavior was found when particles were picked at $t = 4$ Gyr).

Since the potential is changing rapidly at this time, we might expect to observe an enhanced rate of separation of nearby pairs of orbits due to chaos induced by the potential fluctuations provided the e-folding time for this instability is comparable to or greater than that due to the Miller instability. This figure shows, on the contrary, that the initial exponential separation of particles in r at $t = 3$ Gyr does not have a systematically greater slope than the rate of separation of particles at $t = 0$ Gyr. In shell 1 the slope of the dot-dash curve is smaller than that of the solid curve (which we attribute to the fact that heating from the first pericenter passage caused nearby particles to be further apart in phase space); in shell 4 the slopes of all three curves are essentially identical; only in shell 7 is the slope of the dot-dash curve slightly steeper than that of the black curves indicating that chaoticity may be playing a bigger role at large radii.

While this is clearly not conclusive evidence, it is suggestive of the hypothesis that chaoticity due to the time-dependent potential, is not significant compared to the chaoticity due to the Miller instability. It may play a small role in the evolution of the system at larger radii. However there is little evidence to suggest that chaotic mixing from orbits in the time-dependent potential is *driving* the relaxation.

To better understand the mechanism driving the relaxation we now look at separation of particles in energy and angular momentum space. In integrable time-independent potentials, energy and some quantity akin to angular momentum are generally integrals of motion. It is therefore of interest to quantify how these quantities change during a merger.

Figure 4 shows the separations in energies (top panels) and

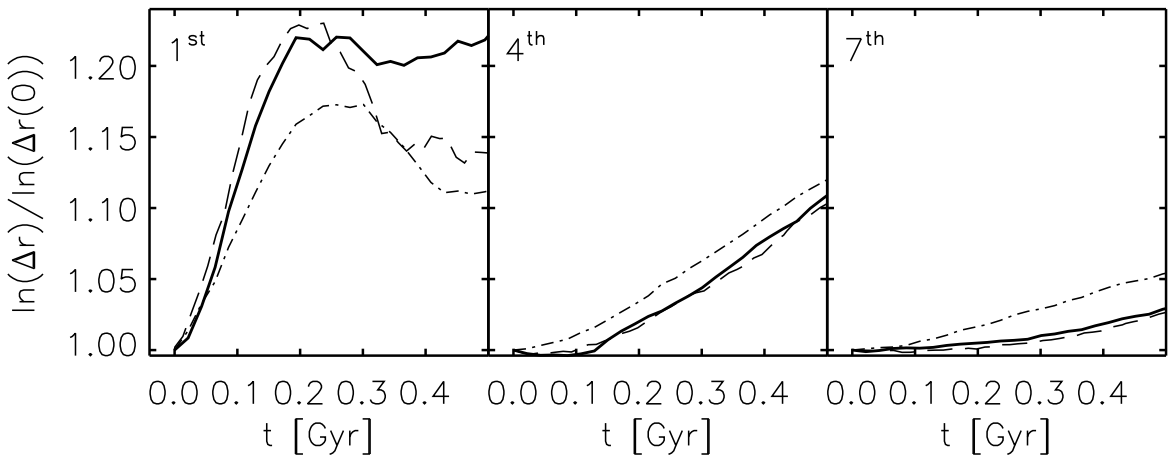

F . 3.— The panels show divergence in the quantities $\ln(\Delta r)/\ln(\Delta r(t=0))$ as a function of time for 1st, 4th, 7th shells. The solid curves are for the merger of two NFW halos (run Bp1) with pairs of particles selected at $t = 0$. Gyr. The dashed curves are for pairs of particles selected at $t = 3.0$ Gyr in the isolated halo and the dot-dashed curves are for pairs of particles selected at $t = 3.0$Gyr. The curves for the pairs starting at $t = 3.0$ Gyr have been translated in time to $t = 0$ Gyr. The dot-dashed curves and the dashed curves indicate that the initial exponential instability of nearby orbits during the merger is not very different from that in the isolated halo, independent of the time at which the particle pairs are selected.

.

angular momentum[6] (bottom panels) for the same pairs of particles as in Figure 2. As before, the dot-dashed lines are for pairs of particles in the isolated halo, while the solid lines are for pairs of particles in one of the merging halos. The quantities $\Delta E, \Delta J$ are scaled relative to their initial values at $t = 0$ Gyr. ΔE and ΔJ (as expected) are very close to zero in the isolated halo[7] .The sharp initial rise in ΔE and ΔJ reflects the response of the particles to the presence of second halo. This a consequence of the fact that although each individual halo is in equilibrium separately, when the two halos are set up on a parabolic trajectory at $t = 0$ they are no longer in equilibrium, since particles now experience the external potential of the second halo.

After the initial increase in ΔE and ΔJ, there are sharp but transient increases in the separation of these quantities that also occurs primarily during pericenter passages. In fact, the peaks in ΔE and ΔJ are strongly correlated with the pericenter passages in all radial shells and provide striking evidence that it is these events that are primarily responsible for scattering particles in E and $\mathbf{J}$. We also note that the step-like changes in these quantities and their correlation with pericenter passages is seen at all radii unlike in the case of Δr and Δv which changed more slowly and continuously in the outer regions. In the inner most shells there is little or no separation in phase-space quantities occurring between pericenter passages. The slight increase in ΔE and ΔJ seen in shell 4 and shell 7 between $t = 2$ Gyr (first pericenter passage) and $t = 5$ Gyr (second pericenter passage) could be evidence for slower chaotic mixing. After the first pericenter passage the outer regions of the two halos never completely separate again and the continued overlap of the two potentials means that at larger radii the tidal compressive field and dynamical friction is able to operate over a longer duration and consequently more gradual changes occur as well. It is clear, however that the impulsive changes in ΔE and ΔJ during multiple pericenter passages have the strongest effect on the mixing in E and $\mathbf{J}$.

Figure 5 compares separations in all four quantities $\ln(\Delta r)$, $\ln(\Delta|v|)$, ΔE and ΔJ for two merger simulations with different numerical resolutions. We recall that the run HRBp was performed with a factor of 10 more particles and approximately a factor of 2 higher force resolution than the run Bp1. We present the comparison for only the innermost shell since this is expected to be the most susceptible to numerical effects, if any. There is clearly very little difference between the overall behavior of separations of particles in any of the 4 quantities plotted. The only noticeable difference is in the initial behavior of $\ln(\Delta r)$, $\ln(\Delta|v|)$.

The insert in the top most panel shows that the initial radial separation of particles in run HRBp is smaller at $t = 0$ Gyr than it is for run Bp1. This is purely a consequence of the fact that by increasing the mass resolution the phase-space coordinates become more densely sampled and this allows us to select pairs of particles that are closer in phase-space (see inserts in top two panels). The insert in the second panel shows that the initial velocity separation ($\ln(\Delta|v|)$) decreases to lower values in run HRBp compared to run Bp1. This also points to the increased gravitational deceleration due to the proximity of the nearest neighbor and the decrease in the softening parameter.

All curves are plotted without scaling them relative to their initial separations to illustrate that apart from differences in the initial separation (which we attribute to the Miller instability), the separations in all four quantities in the different resolution mergers saturate at the same values. This is confirmation that particle separations saturate at values that are determined by the global dynamics of the merger and not by the resolution of the simulations.

Figure 6 shows separations in $\ln(\Delta r)$ and $\ln(\Delta v)$ for particles in different radial shells in run Bp1 and in the merger of an NFW halo with a shallow cusp. The behavior is remarkably similar in both cases except in the innermost shell. This is expected, since the innermost shell is the only one in which the density profiles (and consequently the phase-space den-

[6] The angular momentum (J) is about an axis perpendicular to the plane containing the orbits of the center-of-masses of the two merging halos.

[7] We note that they are not precisely zero because, although the total energy of the system is conserved to within numerical error, the computation of $(\Delta E/\Delta E(t=0))$, E for a given particle is relative to the MBP - which can be a different particle at each time-step.

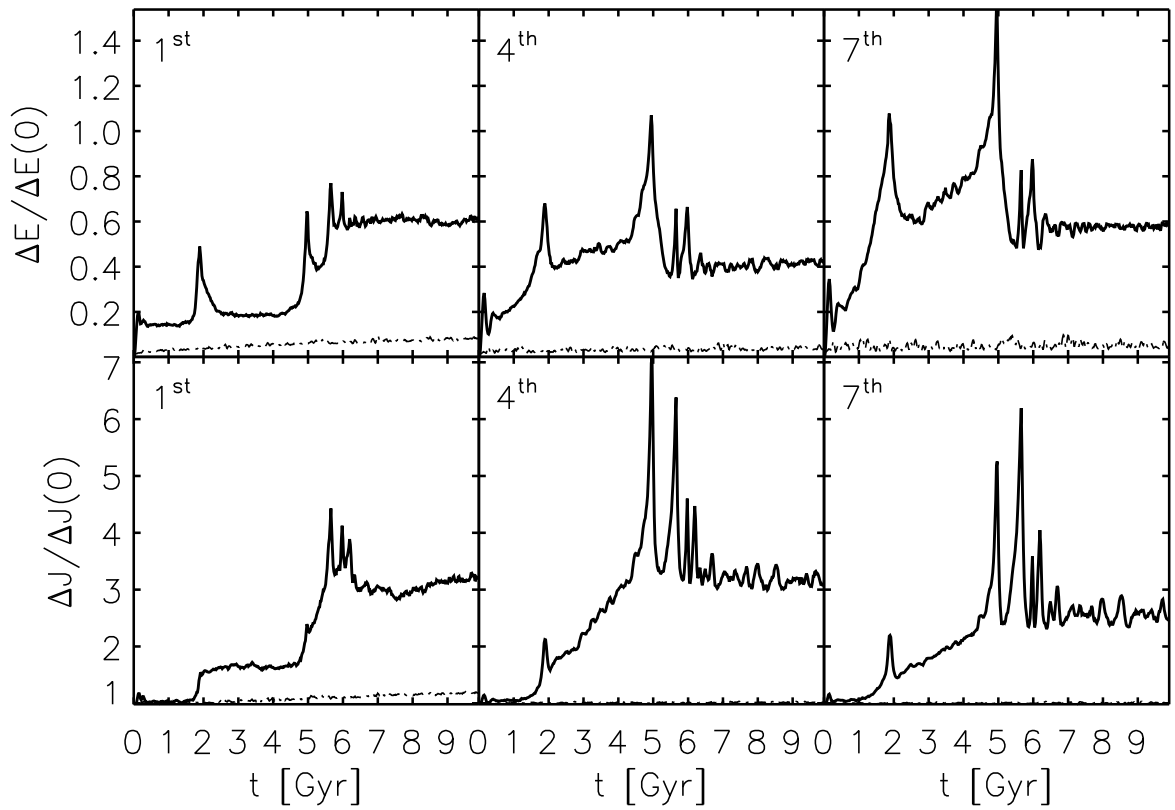

F . 4.— The top three panels show divergence in the quantities $\Delta E/\Delta E(t=0)$ as a function of time for three different shells in the halo (from left to right: the first, fourth and seventh shells respectively). The lower three panels show the quantity $\Delta\mathbf{J}/\Delta\mathbf{J}(t=0)$, for the same three shells. The solid lines are for the merger of two NFW halos (run Bp1). The dot-dashed lines are for the isolated NFW halo.

sity distributions) differ significantly. It is well known from previous studies (Boylan-Kolchin & Ma 2004b; Kazantzidis et al. 2006) that cusps in shallow potentials are less robust than cusps in NFW halos. Particles in the inner most shell of the shallow cusp experience a larger increase in energy due to each pericenter passage than particles in the NFW halo because they experience a greater relative increase in the depth of the external potential arising from the overlap of the two halos, and consequently the phase space volume accessible to them is larger. Beyond the scale radius the two halos have essentially identical density profiles, and separations in $\ln(\Delta r)$ and $\ln(\Delta v)$ are almost indistinguishable.

The results of our investigation of particle separations in $\ln(\Delta r)$, $\ln(\Delta|v|)$, ΔE and ΔJ can be summarized as follows:

1. The initial separation of pairs of nearby particles in N-body systems such as those studied here is a result of the exponential instability of the N-body problem, the so called "Miller instability." The qualitative and quantitative behavior of the separation of particles: e.g. their dependence on local crossing time (Fig. 2), their dependence on softening and force resolution (Fig. 5) are completely consistent with previous studies of this instability. It is important to point out that the very fact that we are able to detect the exponential divergence of orbits due to the Miller instability indicates that despite the fact that pairs of nearby particles in the N-body simulations are separated by macroscopic distances (i.e., are not infinitesimally close by), our method for identifying an exponential instability can be applied successfully to an N-body system.

2. Subsequent to the saturation of the separations due to the Miller instability, the most significant increase in separations of nearby particles (in r, v, E, or $\mathbf{J}$) occur during pericenter passages of the MBP of the two halos and is a consequence of the compressive tidal shocking (due to the overlap of the two halos) and dynamical friction between the two halos that occurs during the pericenter passages. In the innermost shells there is little or no separation in phase-space quantities occurring between pericenter passages, despite the large global fluctuations in potential occurring during these times. At larger radii separation in r, v continue following pericenter passages. At larger radii, there is also a small (but short lived) increase in separation in E and J between the first and second pericenter passages.

3. If we consider the increase in the macroscopic separation of particles in (r, v) to be a measure of the mixing of particles in these quantities, these plots would lead us to conclude that the majority of mixing occurs due to the Miller instability and several phases of mixing that occur during pericenter passages of the two halos. In all radial shells of merger simulation we observe that the macroscopic separation of initially nearby particles increases until it saturates. In the merging halos, saturation occurs at larger values of $\ln(\Delta r)$, $\ln(\Delta|v|)$ respectively, than in the isolated halo. This is a consequence of the fact that the accessible phase-space volume has

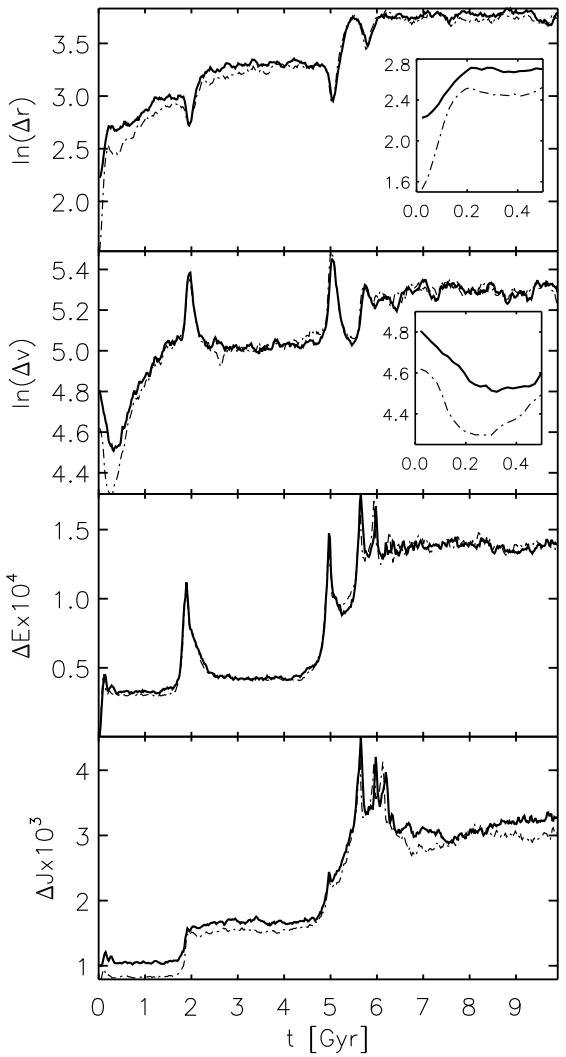

F . 5.— The four panels (top to bottom) show divergence in the four quantities $\ln(\Delta r)$, $\ln(\Delta|v|)$, ΔE and ΔJ plotted as a function of time for pairs of particles in the innermost shell of one of the two merging NFW halos. The solid lines are for the merger of two halos with 2×10^5 particles in each halo (run Bp1); dot-dashed lines are for the merger of two halos with 2×10^6 particles in each halo (run HRBp). The inserts in the top two panels show differences in the initial separation due to the Miller instability. The dot-dash line starts at lower values in both $\ln(\Delta r)$, $\ln(\Delta|v|)$ which is a result of picking particles closer in phase space in run HRBp. For run HRBp $\ln(\Delta r)$ has a shorter e-folding time, due to the higher particle number and smaller softening length. Apart from the behavior of initial separations in all four quantities, the low and high resolution mergers are almost identical.

increased during the merger process. We saw from Figure 4 that ΔE and ΔJ (which represent increases in the available phase-space states accessible to particles) increased in step-wise fashion primarily during pericenter passages of the MPBs, as was predicted by Spergel & Hernquist (1992). By $t = 7$ Gyr the virial ratio $2T/|V| \approx 1$, although the potential continues to experience long-lived but low-amplitude oscillations until 13 Gyr. The low-level potential fluctuations cause little change in the separation of either r or v beyond 7 Gyr.

In Lynden-Bell's (1967) model for "violent relaxation", particles experience changes in their phase-space coordinates due to their interaction with a time-varying background potential. It has been argued by various authors that a time-dependent potential alone is inadequate to cause relaxation, since nearby particles in phase space will merely be relabeled in energy and will not separate (or mix). The results from this section indicate that during the merger of two halos, nearest neighbor particles in phase space do mix in E and $\mathbf{J}$. Further, the primary causes of mixing are the compressive tidal shocks and dynamical friction which transfer energy and angular momentum from the orbital motion of the two merging halos to the particles during the pericenter passages (Spitzer & Chevalier 1973; Gnedin et al. 1999; Valluri 1993). The particles respond to sudden increments in their orbital energy and angular momentum by jumping to new orbits, resulting in mixing in phase space and evolution to a new distribution. This latter phase of evolution could indeed be the result of some weaker form of chaotic mixing, coupled with phase mixing, both of which occur on a longer timescale.

3.2. *Mixing of ensembles in phase-space*

In this section we present results of the mixing experiments with an initially coherent ensemble of particles selected from the N-body simulation. As discussed in 2.3.2 we confine our analysis to mixing in the scaled energy and angular-momentum variables $\mathcal{E}, \mathcal{J}$.

Figure 7 shows the evolution of an ensemble of 1000 self-gravitating particles in the 4th shell in run HRBp. The density contours are obtained using a kernel smoothing algorithm. At $t = 2$ and $t = 5$ Gyr which correspond to the first and second pericenter passage, respectively, the ensemble undergoes a sudden spreading in energy ($\mathcal{E}$) which is a consequence of the deepening of the potential during the overlap of the two halos. By $t = 6$ Gyr the particle distribution fills a triangular region in $\mathcal{E}, \mathcal{J}$ space. A greater spreading in $\mathcal{E}$ at the smallest values of angular momentum is a consequence of the fact that these orbits are on the most radial orbits and consequently experience greater changes in their potential energies. Particles with the smallest (most negative) values of $\mathcal{E}$ experience the greatest spread in angular momentum largely as a consequence of their being ejected during the tidal shocks to larger radii.

We carried out similar mixing experiments for over 25 different ensembles in each shell. The behavior of the ensemble in Figure 7 was found to be quite representative of all the different ensembles.

Figure 8 shows contours of projected density of particles as a function of the quantities $(\mathcal{E}, \mathcal{J})$ in run HRBp, for ensembles in 3 different radial shells at 4 different times in the evolution. The evolution of the ensembles in shells 1, 4 and 7 are very similar. At $t = 2$ Gyr (first pericenter passage) the ensemble spreads in $\mathcal{E}$. Similar increases in spread and are seen during the 2nd pericenter passages (but are not shown here). After the first pericenter passage the majority of the particles in the ensemble at $t = 4$ Gyr return to a more compact distribution in $(\mathcal{E}, \mathcal{J})$ but one with a larger spread in $\mathcal{J}$ at small $\mathcal{E}$. The bottom panels correspond to $t = 6$ Gyr, after the first three pericenter passages have occurred. At this time all the ensembles fill a roughly triangular region in $\mathcal{E}, \mathcal{J}$ space. This characteristic triangular final distribution is seen in all shells and for essentially all of over a hundred different ensembles we examined. This final distribution is not uniform in density, but the density contrast across the ensemble is much smaller than in the initial distribution. We note that when these ensembles were re-observed at 15 Gyr there was slightly greater

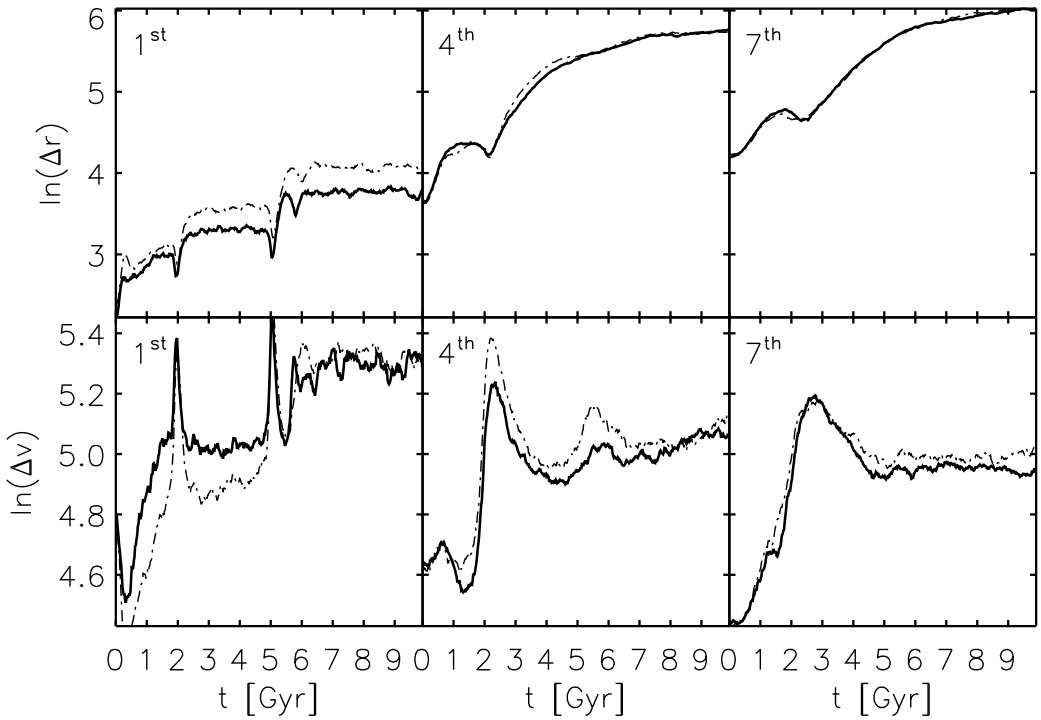

F . 6.— Solid lines show separations in ln(Δr) and ln(Δv) for the merger of two NFW halos and the dot-dash lines show the separations of these quantities for the merger between an NFW halo and a halo with an inner shallow cusp of $\gamma = 0.2$. The behavior is similar in both cases except in the innermost shell where the differences in the density profiles are significant.

uniformity of density in the lower-density tails but otherwise they had changed very little from their distributions at 8 Gyr.

There are two important observations that can be made: (a) changes in $\mathcal{E}, \mathcal{J}$ occur primarily during pericenter passages (Fig. 7) , and (b) the final distribution in $\mathcal{E}, \mathcal{J}$ space of the ensembles at all radii are similar, and the rate at which this final distribution is reached is independent of radius (Fig. 8).

The mean crossing time in the innermost shell ($r \leq 25$ kpc) is $\sim 5 \times 10^8$ yrs, while in the 7th shell is ~ 6.5 Gyr. It is obvious from Figure 8 that although the crossing time in shell 7 is a factor of 10 longer than in shell 1, the diffusion of the ensembles in $(\mathcal{E}, \mathcal{J})$-space appears to occur primarily due to the pericenter passages of the MBPs and there is only a slightly increased rate of spreading at larger radii. Phase mixing and chaotic mixing in isolated potentials occur at rates that scale with the local dynamical time so one would expect that mixing effects that depend on the local dynamical time (such as chaotic mixing) would occur faster at small radii than at large radii. The fact that the evolution of the ensembles at different radii occur episodically following pericenter passages, rather than continuously at a rate that scales with local orbital time points to the importance of the impulsive tidal events as the processes that drives the transition to an equilibrium distribution in energy and angular momentum.

Indeed, the absence of a strong dependence on local crossing time in Figure 8 provides the strongest evidence so far that mixing in energy and angular momentum is driven by compressive shocking and dynamical friction that occur at pericenter passages. While chaotic mixing, as defined for static smooth potentials, might be occurring during the merger of two halos, it plays a minor role in driving the remnant to equilibrium.

4. INCOMPLETE RELAXATION AND REDISTRIBUTION OF PARTICLES IN MERGERS

Two interesting aspects of merger simulations of DM halos that have been pointed out recently are (a) that cusps are remarkably robust and (b) that about 40% of the total mass of the remnant lies beyond fiducial virial radius (Kazantzidis et al. 2006). Two questions that arise from these findings are: 1) how do the final radial distributions, energies and angular momenta of particles in the remnant depend on their original location in the merging halos and, 2) From where do the particles that end up outside the virial radius in the merger remnant originate? Addressing the first question is important since the merger causes the redistribution of particles to occur in a way that the density profiles and phase-space distribution functions preserve homology. This may be interpreted as an indication that particles at all radii are being heated uniformly at all radii. However, it is also reasonable to assume that less bound particles in the outer part of the halo are preferentially heated.

It is also of interest to understand how the relative change in energy or angular momentum of particles depends on their initial location in the halo. In this section we examine the redistribution of particles in radius, energy and angular momentum and the dependence of their final locations on their initial location in the merging halos. We note in passing that while the isolated halos and the initial merging halos are spherical, justifying the use of spherical radial shells, the merger remnant is significantly prolate-triaxial with minor-to-major principal axis ratio c/a varying from 0.5 at the center to 0.7 at the virial radius. Although the merger remnants exhibit significant departures from spherical symmetry, in what follows we ignore the triaxiality of the final distribution when binning particles in radius.

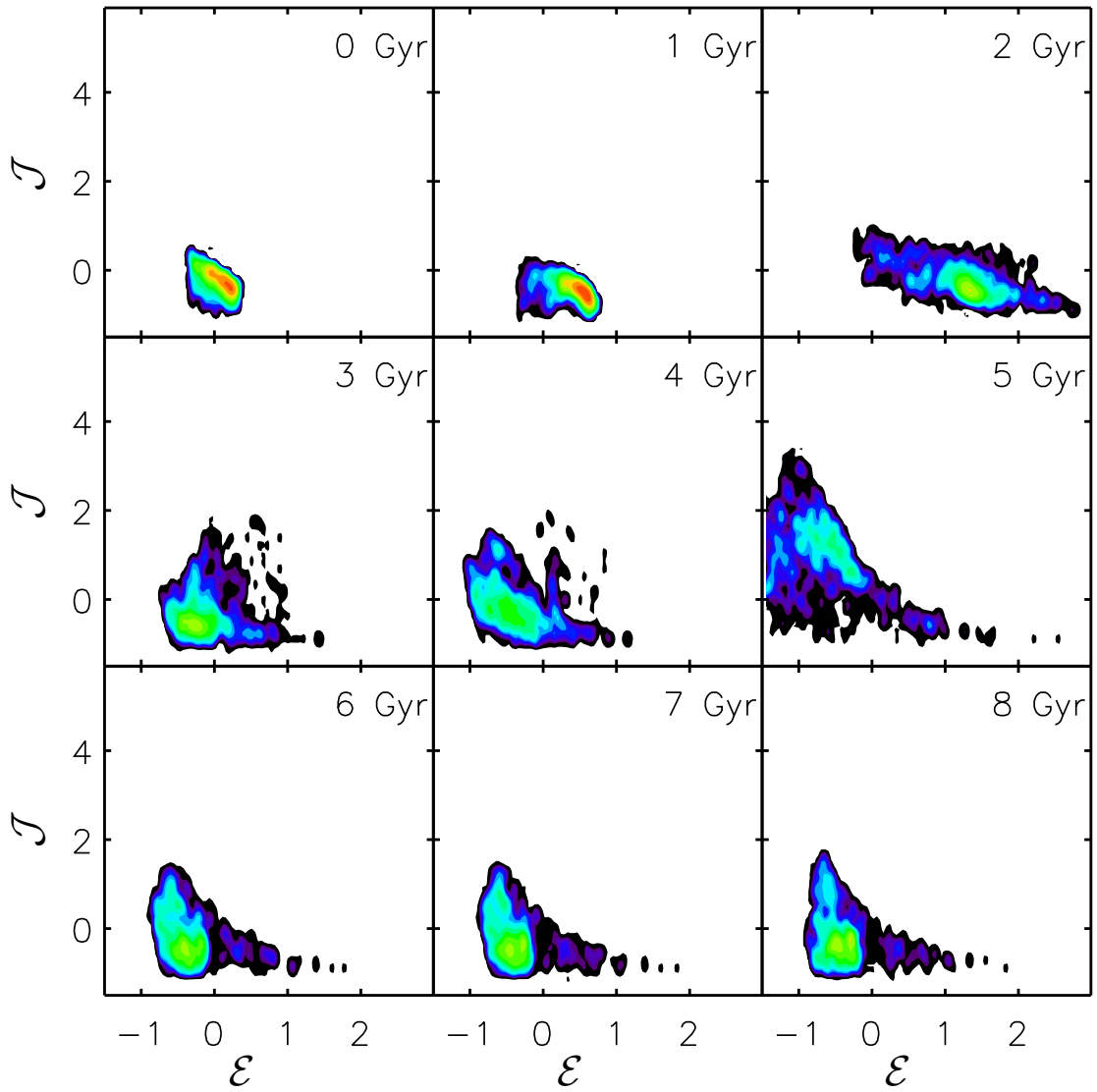

F . 7.— The evolution of an ensemble of 1000 nearest neighbors in phase-space in shell 4 at $t = 0$ (run HRBp) plotted at 1 Gyr time intervals in the merger. The plot shows isodensity contours for the particle distribution. The red contours correspond to the highest density regions and black to the lowest density regions. The contours are spaced at logarithmic density intervals relative to the maximum density contour to enhance the visibility of low density regions. Pericenter passages (at $t = 2$ and $t = 5$ Gyr) are seen to cause a sudden spreading of the entire ensemble in $\mathcal{E}$ (a result of the tidal shocking at these times). Two additional pericenter passages occur between $t = 5 and t = 6$ (see Fig. 1). By $t = 6$ Gyr the ensemble has experienced 4 pericenter passages and has settled to fill a triangular region in the $\mathcal{E}, \mathcal{J}$ space.

Each panel in Figure 9 shows how particles that were originally in a given shell (indicated by the caption) are redistributed in the final radial shells at $t = 9$ Gyr when the merger would conventionally be deemed complete. The results for isolated halo are an important baseline for comparison.

In the top panel (shell 1), the solid lines (merger) and dot-dash lines (isolated halo) are remarkably similar but indicate that while the cusp is quite robust, in fact as much as 20% of the particles in the isolated halo and over 40% of the particles in the merging halos end up outside the cusp at the end of the simulation. The primary reason is that 80% of the particles in the isolated halo have apocenters within the cusp. The merger only causes a small additional fraction (20%) of these bound particles to be spread to shells immediately outside the cusp (shells 2-4). In comparison with the outer shells, this level of redistribution for shell 1 is somewhat modest.

The middle panel (shell 4) shows that, for the isolated NFW halo (dot-dashed curve), $\sim$ 50% of the particles are in shells 3 and 4 at the end of the simulation, but the remainder are almost uniformly redistributed within shells 2, and 5-10. In shell 7 of the isolated halo $\sim$ 45% of the particles stay in shells 6 and 7 while the remainder are redistributed almost uniformly to all radii from shell 4 outward. Thus, there is significant radial redistribution of particles even in the non-evolving isolated NFW halo purely because the initial distribution function has an isotropic velocity distribution with roughly equal fractions of radial and tangential orbits. The peaks in shells (3,4) and (6,7) are due to the more tangentially biased orbits. A comparison of the dot-dash curves with the solid curves shows that the main effect of the merger is to flatten out the peaks due to tangential orbits thus making the final distributions more radially anisotropic. At all radii the merger is responsible for redistributing about $\sim 15 - 20\%$ more particles from a given bin to other radial bins.

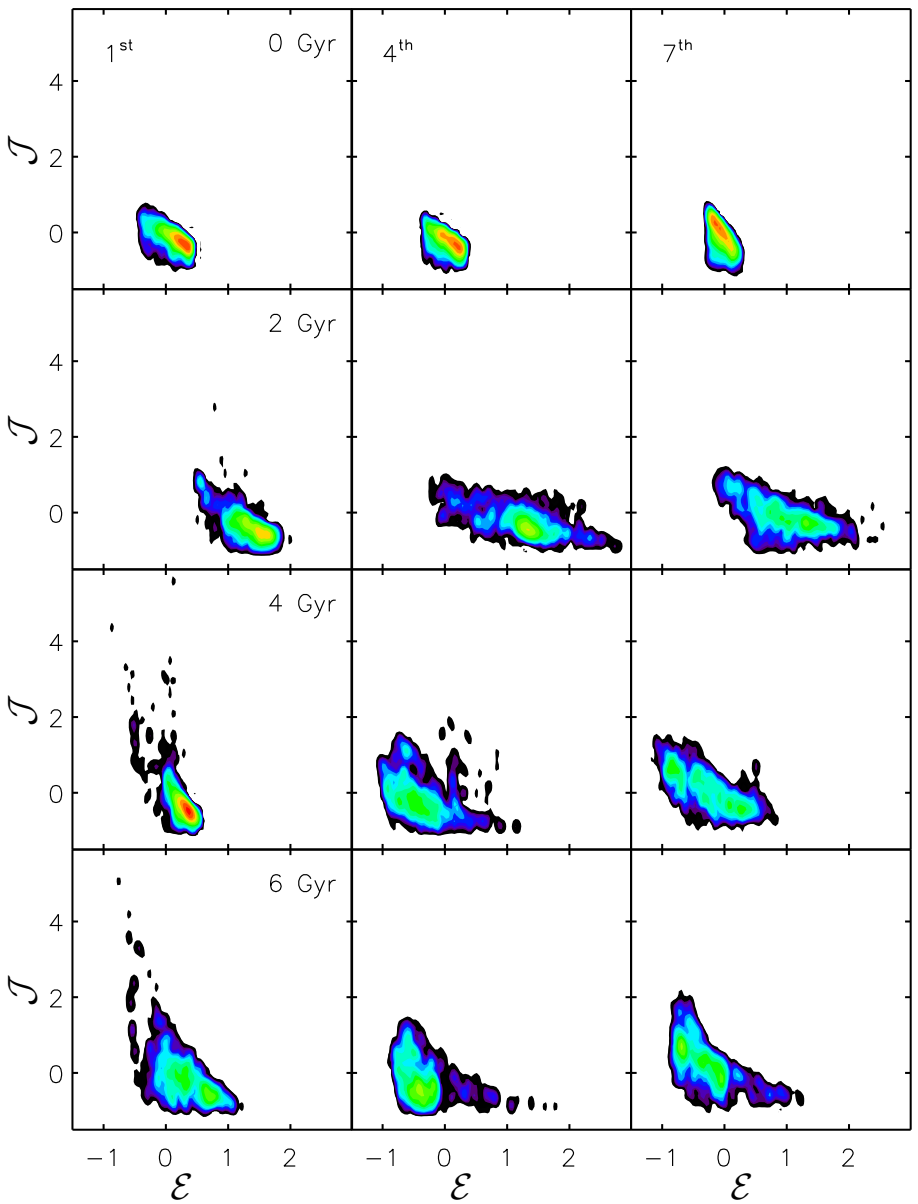

F . 8.— Isodensity contours for ensembles of particles plotted as a function of $\mathcal{E}, \mathcal{J}$ for shell 1(left hand column), shell 4(middle column) and shell 7(right-hand column) plotted for different times in their evolution (see text for details).

A similar study of the merger of a NFW halo with a halo having a shallow cusp showed that except in the innermost shell where the profiles of the two halos differ, the particles in the two halos with cusps of different slope are redistributed identically. A larger fraction ($\sim$ 45%) of particles in the shallow cusp were redistributed by heating to radial shells (2-4) directly outside the cusp (in comparison with 20% in NFW-NFW halo mergers). The differences in the distribution of particles at the end of the merger confirm that NFW cusps are robust and retain a much more significant fraction of their particles than do shallow cusps, confirming what has been previously found by other authors (Boylan-Kolchin & Ma 2004b; Kazantzidis et al. 2006).

Figure 10 shows distributions of the changes in the kinetic, potential, and total energies of all particles in different shells at the end of the merger ($\Delta E = E_{\rm final} - E_{\rm initial}$). Particles in the innermost shell experience a net decrease in total energy that is a result of the overall decrease in the potential energy of the particles pointing to an energy segregation phenomenon during mergers (Funato et al. 1992). This is expected, since there is an overall increase of $\sim$ 60% in the mass of the cusp compared to the mass in the initial cusp (Kazantzidis et al. 2006). At all other radii, there is a net increase in total energy that is most significant at larger radii. This is a result of significant fractions of particles gaining potential energy and being redistributed to larger radii as seen from the multiple peaks in the potential energy distributions arising from particles heated during each pericenter passage. It is striking to note that in all shells the kinetic energy distributions remain peaked about $\Delta E = 0$ and are more peaked than Gaussian, indicating that the majority of particles experience only a small change in their kinetic energies despite experiencing large changes in their potential energies. This is additional confirmation that the redistribution in energy that we saw in the mixing experi-

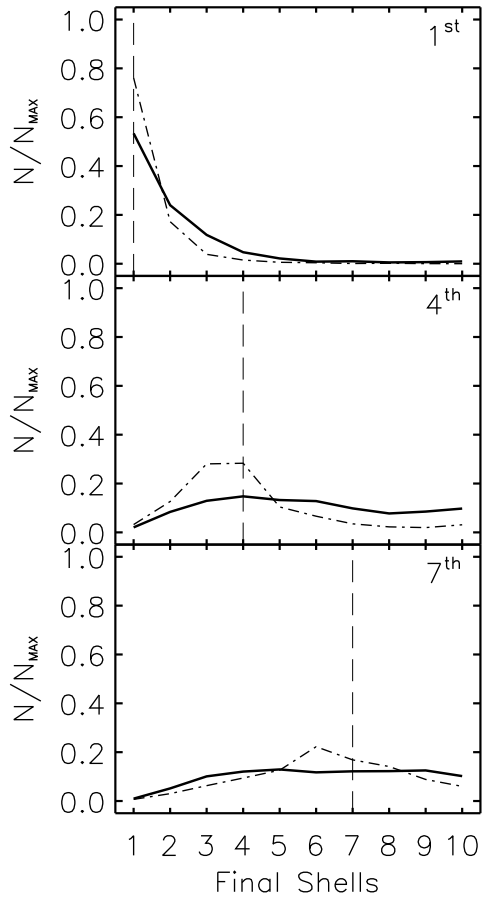

F . 9.— The fraction of particles ($N/N_{\rm max}$) that lie in each of the radial shells at the final time step. The vertical dashed line and the caption in each panel indicate the shell in which particles were at t = 0 Gyr. Particles from one of the two NFW halos (in run Bp1) is shown as a solid line while particles in the same shells of the isolated NFW halo are shown by dot-dashed line.

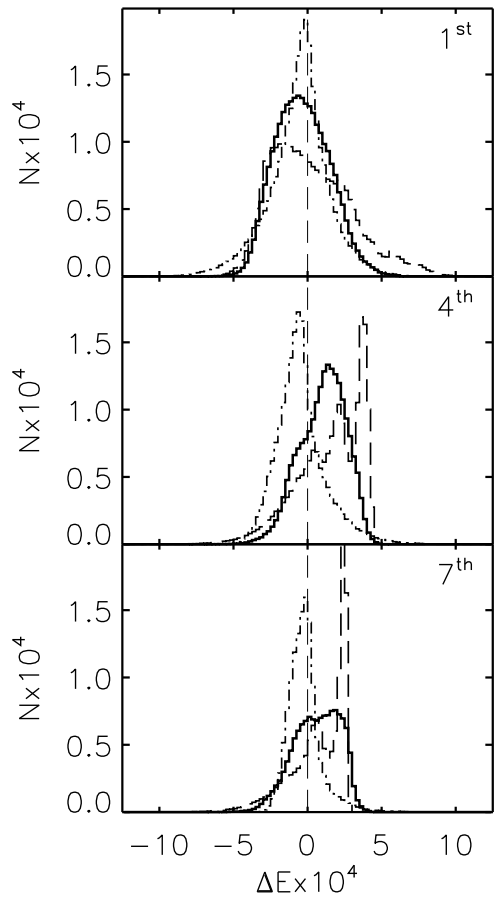

F . 10.— Histograms of the change in energy ($\Delta E = E_{\rm final} - E_{\rm initial}$) for all particles in shells 1 (top), 4 (middle), and 7 (bottom). The solid line shows the change in total energy, the dot-dashed shows the change in kinetic energy, and the dashed line shows the change in potential energy.

ments (§3.2) is primarily due to changes in potential energies of particles due to interactions with the background potential during pericenter passages.

The innermost shell includes all particles within $\sim$ 25 kpc, which is slightly larger than the initial scale radius (r_s = 21 kpc) of the merging NFW halos. Figure 11 is similar to Figure 10 but shows how particles in three equal radial shells within r_s are redistributed in energy. It is clear that the particles in the inner 33% of the scale radius experience the greatest deepening in the potential.

Figure 12 shows histograms of change in J_z (the component of **J** perpendicular to the orbital plane of the merger) for all particles in radial shells 1, 4 and 7. The highly peaked distributions in the innermost shell indicates that there is virtually no net change in J_z for the particles here. In the outer two shells, ΔJ_z has an increasingly wider distribution. Although it is not plotted here, we note that in the outermost shells (shells 9, 10) the median of the distribution of ΔJ_z shifts to slightly positive values, indicating a small gain in net angular momentum for the outermost particles. The observed increase is a result of transfer of the orbital angular momentum of the merging halos into the angular momentum of individual particles. Our results indicate that the angular momentum of the merger is absorbed primarily by particles at large radii.

As was noted previously, about 10% of the mass of the initial DM halos lies outside the fiducial virial radius, but it has been found that nearly 40% of the mass of the final remnant lies outside the virial radius of the remnant halo (Kazantzidis et al. 2006). We now examine the distribution of particles in the merger remnant of run Bp1 to determine where these particles originate from. Figure 13 shows the fraction ($F_{\rm vir}$) of the total number of particles lying beyond the virial radius of the remnant that originated from each of the 10 shells of the original halos. All particles that lay outside the virial radius in the original halos are assigned to shell 11 (which extends from the virial radius to the outer edge of the simulation volume). The highest fraction (about 25%) of the particles outside the virial radius of the remnant were already outside the virial radius of the initial systems. The innermost shell is the most robust with fewer than (< 1%) being ejected beyond $R_{\rm vir}$, Interestingly, all shells from the half mass radius onward (shell 3 and beyond) contribute roughly equally ($\sim 8-11\%$) to the particles that lie outside $R_{\rm vir}$ in the final remnant. This figure and Figure 9 together show that the radial redistribution of particles occurs essentially independently of the original radius of the particle, provided that the particles lie outside the central 3 shells.

These results further highlight the fact that mass, in its standard virial definition, is not additive in mergers. Models in which the mergers double the mass within the virial radius of

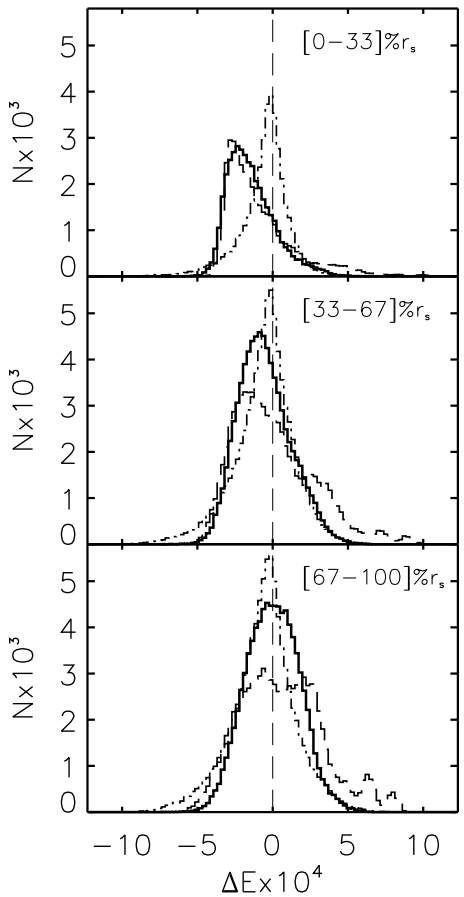

F . 11.— Histograms of the change in energy ($\Delta E = E_{\rm final} - E_{\rm initial}$) for all particles in three equal radius bins within the scale radius (r_s = 21 kpc). The solid line represents total energy, the dashed-dot represents kinetic energy and the dashed represents potential energy.

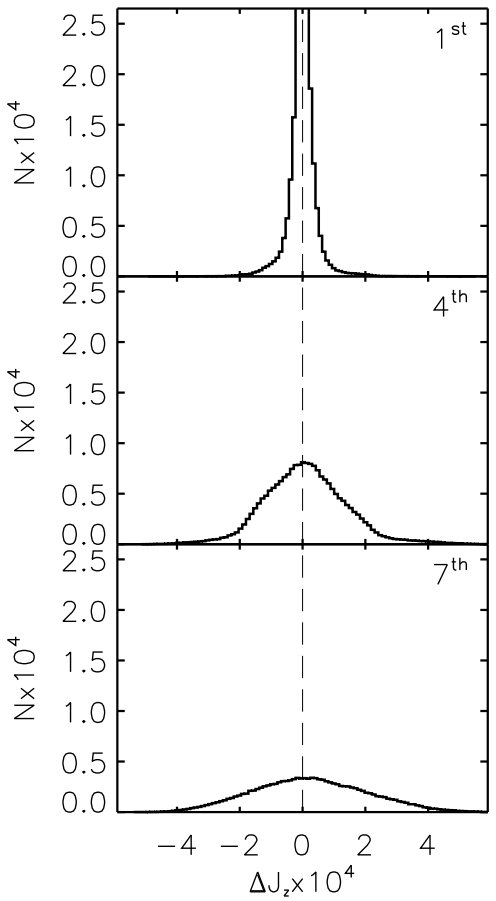

F . 12.— Histograms of change in J_z (component of **J** perpendicular to the orbital plane of the merger) for all particles in the selected shells.

the remnant greatly overestimate both the mass and density of the merger product.

5. SUMMARY AND DISCUSSION

The principal goal of this study was to investigate the processes that drive the evolution of self-gravitating systems to equilibrium and cause mixing in phase-space. The goal was also to determine whether the possible presence of large fractions of chaotic orbits arising from the time-dependent potential was responsible for driving the system to equilibrium. We summarize the main results below.

1. All orbits in the *N*-body simulation exhibit the well-documented "Miller instability" of the *N*-body problem. This instability results in an initial nearly exponential separation of nearby orbits in configuration space and energy, and a decrease in velocity separation. The *e*-folding time (t_e) for the separation increases with increasing softening length and decreasing particle number. The initial exponential separation saturates on a short timescale ($\sim 5t_e \sim 0.25$ orbital crossing times) and remains constant thereafter. The *e*-folding time and the rate at which the instability saturates are identical in the merging and isolated halos indicating that this is purely a consequence of the *N*-body nature of the problem and not a result of the merger. To this end, we use control simulations of isolated halos as a baseline for comparison with merging halos to identify the mixing processes occurring in mergers.

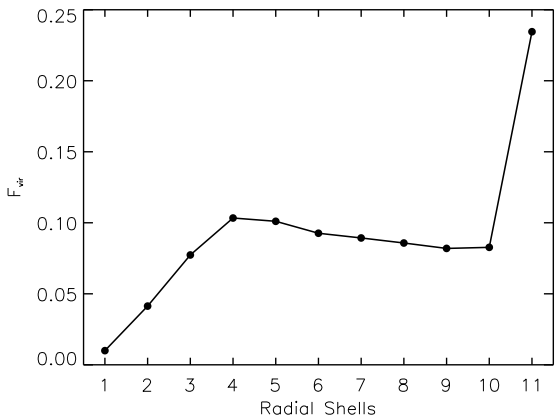

F . 13.— Fraction of particles that originated in each of the radial shells (1-11) in one of the original NFW halos involved in the merger that end up outside the fiducial virial radius of the remnant. (All particles beyond the virial radius are assigned to shell 11.)

2. After the initial growth in $\ln(\Delta r)$ and decrease in $\ln(\Delta|v|)$, there are periods of time for which these quantities are almost constant, separated by several sharp decreases in $\ln(\Delta r)$ and correspondingly sharp peaks in $\ln(\Delta|v|)$ that are not seen in the isolated halo. The transient changes in $\ln(\Delta r)$ and $\ln(\Delta|v|)$ are coincident with each other and correspond to the pericenter passages of the centers of the merging halos. Pericenter passages also cause sharp transient step-like changes in the energy and angular momentum separation of pairs of particles. Between pericentric passages there is very little evidence for for mixing in the innermost shell, but at larger radiiln(Δr) and $\ln(\Delta|v|)$ continue to grow slowly with time due to the overlap of the merging halos.

3. The changes in ΔE and ΔJ are more strongly correlated with pericenter passages at all radii pointing to the importance of compressive tidal shocks. At larger radii there are is also some growth in separation between pericentric passages, possibly pointing to the continued action of chaotic mixing. If we assume that separations of nearby particles in phase-space are linked to "mixing", this implies that the principal drivers of strong mixing are the compressive tidal shock and increased dynamical friction that occurs during the pericentric passages.

4. Mixing experiments with ensembles of 1000 nearest particles in phase-space showed that mixing in the phase-space variables $\mathcal{E}, \mathcal{J}$ also occurs primarily during pericenter passages. Mixing leads ensembles of nearby self-gravitating particles to spread and fill a triangular region in $\mathcal{E}, \mathcal{J}$ space. Mixing in these parameters occurs at the same rate at all radii, largely independent of the characteristic crossing time of the ensemble. This is further evidence that the mixing process is driven by pericentric passages and is unrelated to mixing processes that scale with the local crossing time.

5. We confirm the findings of several other authors that cusps of DM halos are remarkably robust. The robustness of cusps is a consequence of the fact that 80% of the particles in the first shell have apocenters that lie within the first shell. During the merger only a small fraction (20%) of particles with apocenters within the original cusp are ejected to larger radii. The majority of the ejected particles do not get beyond shell 4. A much larger fraction ($\sim 45\%$) of particles in the central regions of core-like profiles is ejected to radial shells directly outside the cusp during a merger.

6. Particles in a given radial shell outside the cusp are redistributed almost uniformly with radius primarily due to phase mixing. This result holds for both the isolated spherical halo and the merging halos. The merger helps to redistribute an additional ~20% of orbits that have predominantly tangential velocity distributions in the original halos.

7. Particles within the scale radius of the merging NFW halos experience a net decrease in total energy following the merger. This is a result of the overall decrease in the potential energy of the particles, resulting from the ($\sim 60\%$) increase in the mass of the cusp in the final remnant.

8. The majority of particles in the merging halos experience only a small change in their kinetic energies and moderate changes in their potential energies. The change in total energy of particles is driven predominantly by the changes in their potential energies during pericenter passages.

9. At smaller radii the majority of particles experience only small change in angular momentum evidenced by highly peaked distributions of ΔJ. The angular momentum of the merger is absorbed primarily by particles in the outermost radial shells.

10. The largest fraction of particles lying beyond the virial radius of the final remnant (25%) were located beyond the virial radius of the original halos. The inner 2 shells are most robust to the ejection of particles beyond the virial radius. All shells between shell 4 and the virial radius (shell 10) contribute roughly equally to the particles ejected beyond $R_{\rm vir}$ of the remnant.

While this paper focuses on simulations of the merger of two dark matter halos with NFW potentials, most of the results are generic to mergers of collisionless gravitating systems and therefore applicable to dissipationless ("dry") mergers of elliptical galaxies. In particular, the absence of large amounts of mixing in radius over and above that expected from phase mixing in an isolated halo suggests that radial gradients in stellar properties (such as metallicity gradients) are likely to survive intact even in major mergers. The robustness of cusps in the merger suggests that stellar cusps such as the recently discovered compact nuclear star clusters ("massive compact objects") in low and intermediate luminosity early type galaxies in the Virgo cluster (Ferrarese et al. 2006) might point to the absence of the apparently ubiquitous supermassive black holes in these systems since black holes may reasonably be expected to destroy such cusps by tidally unbinding a compact star cluster.

Finally, we find strong evidence that the processes that drive the mixing in phase space and evolution to a dynamical equilibrium do not occur continuously due to the time-dependent potential of the system. In fact strong mixing occurs primarily following episodic injection of energy and angular momentum into the internal energies of particles during pericenter passages. The injection of energy and angular momentum causes nearest particles in phase-space to separate in $E, \mathbf{J}$.

Previous studies of orbital evolution in time-dependent and time-independent potentials have argued that the presence of large fractions of chaotic orbits could be the principal driver of the mixing and evolution to an equilibrium distribution. While chaotic mixing could well be occurring, we do not find evidence that such chaotic mixing is driving the relaxation. This is probably a consequence of the fact that the timescales required for chaotic mixing to be relevant are much longer than the duration of the merger.

Two interesting questions remain regarding "violent relaxation": 1) does the mixing that occurs during collapse of an isolated cold gravitating system give rise to similar mixing in phase-space? 2) what gives rise to the universal power-law phase-space density profiles seen in cosmological mergers? We defer addressing both questions to future work.

We would like to acknowledge the inspiration provided by the late Henry Kandrup (who was IMV's thesis advisor at the

time of his death) and his significant contributions to this subject. This work has been greatly influenced by his legacy. We thank D. Merritt, R.H. Miller, I.V. Sideris, C. Siopis, S. Tremaine, P. Vandervoort and T. de Zeeuw for detailed comments on an earlier draft of this paper. MV is supported by the Kavli Institute for Cosmological Physics (KICP) at the University of Chicago. IMV acknowledges the support of National Science Foundation (NSF) grant AST-0307351 to the University of Florida and the support of Northern Illinois University and KICP. SK is supported by the Swiss National Science Foundation and by the KICP. AVK is supported by NSF under grants AST-0507666 and AST-0239759, and by NASA through grant NAG5-13274. CLB is supported by the Department of Energy through grant DE-FG02-04ER41323 to NIU. This work used the resources and support of KICP which is funded by NSF through grant PHY-0114422. The numerical simulations used in this study were performed on the zBox1 supercomputer at The University of Zürich. This research made use of the NASA Astrophysics Data System.

REFERENCES

Aarseth, S. J. & Lecar, M. 1975, ARA&A, 13, 1
Arad, I., Dekel, A., & Klypin, A. 2004, MNRAS, 353, 15
Arad, I. & Johansson, P. H. 2005, MNRAS, 362, 252
Arad, I. & Lynden-Bell, D. 2005, MNRAS, 361, 385
Ascasibar, Y. & Binney, J. 2005, MNRAS, 356, 872
Binney, J. 1977, MNRAS, 181, 735
Binney, J. & Tremaine, S. 1987, Galactic dynamics (Princeton, NJ, Princeton University Press, 1987, 747 p.)
Boylan-Kolchin, M. & Ma, C.-P. 2004a, MNRAS, 349, 1117
—. 2004b, MNRAS, 349, 1117
Chandrasekhar, S. 1943, Reviews of Modern Physics, 15, 1
Dehnen, W. 2005, MNRAS, 360, 892
Del Popolo, A. 2003, A&A, 406, 1
Dubinski, J. & Carlberg, R. G. 1991, ApJ, 378, 496
Ferrarese, L., Côté, P., Dalla Bontà, E., Peng, E. W., Merritt, D., Jordán, A., Blakeslee, J. P., Haşegan, M., Mei, S., Piatek, S., Tonry, J. L., & West, M. J. 2006, ApJ, 644, L21
Fujii, M., Funato, Y., & Makino, J. 2006, PASJ, 58, 743
Funato, Y., Makino, J., & Ebisuzaki, T. 1992, PASJ, 44, 291
Gnedin, O. Y., Lee, H. M., & Ostriker, J. P. 1999, ApJ, 522, 935
Goodman, J., Heggie, D. C., & Hut, P. 1993, ApJ, 415, 715
Graham, A. W., Merritt, D., Moore, B., Diemand, J., & Terzic, B. 2005, ArXiv Astrophysics e-print: astro-ph/0509417
Habib, S., Kandrup, H. E., & Mahon, M. E. 1997, ApJ, 480, 155
Hemsendorf, M. & Merritt, D. 2002, ApJ, 580, 606
Hut, P. & Heggie, D. C. 2001, ArXiv Astrophysics e-print: astro-ph/0111015
Jiang, I.-G. & Binney, J. 2000, MNRAS, 314, 468
Kandrup, H. E., Mahon, M. E., & Smith, H. J. 1994, ApJ, 428, 458
Kandrup, H. E., Pogorelov, I. V., & Sideris, I. V. 2000, MNRAS, 311, 719
Kandrup, H. E. & Sideris, I. V. 2001, Phys. Rev. E, 64, 056209
—. 2003, ApJ, 585, 244
Kandrup, H. E. & Siopis, C. 2003, MNRAS, 345, 727
Kandrup, H. E. & Smith, H. J. 1991a, ApJ, 374, 255
—. 1991b, ApJ, 374, 255
Kandrup, H. E., Vass, I. M., & Sideris, I. V. 2003, MNRAS, 341, 927
Kazantzidis, S., Magorrian, J., & Moore, B. 2004a, ApJ, 601, 37
Kazantzidis, S., Mayer, L., Mastropietro, C., Diemand, J., Stadel, J., & Moore, B. 2004b, ApJ, 608, 663
Kazantzidis, S., Zentner, A. R., & Kravtsov, A. V. 2006, ApJ, 641, 647
Kravtsov, A. V., Gnedin, O. Y., & Klypin, A. A. 2004, ApJ, 609, 482
Laskar, J. 1990, Icarus, 88, 266
Laskar, J., Froeschlé, C., & Celletti, A. 1992, Physica D Nonlinear Phenomena, 56, 253
Lichtenberg, A. J. & Lieberman, M. A. 1992, Regular and Chaotic Dynamics. (Applied Mathematical Sciences, New York: Springer, 1992)
Lynden-Bell, D. 1967, MNRAS, 136, 101
Mahon, M. E., Abernathy, R. A., Bradley, B. O., & Kandrup, H. E. 1995, MNRAS, 275, 443
Merritt, D. 2005, ArXiv Astrophysics e-print: astro-ph/0502169
Merritt, D., Navarro, J. F., Ludlow, A., & Jenkins, A. 2005, ApJ, 624, L85
Merritt, D. & Quinlan, G. D. 1998, ApJ, 498, 625
Merritt, D. & Valluri, M. 1996, ApJ, 471, 82
Miller, R. H. 1964, ApJ, 140, 250
Navarro, J. F., Frenk, C. S., & White, S. D. M. 1996, ApJ, 462, 563
—. 1997, ApJ, 490, 493
Sideris, I. V. 2004, Celestial Mechanics and Dynamical Astronomy, 90, 147
—. 2006, Physical Review E (in press), 73, 1
Sideris, I. V. & Kandrup, H. E. 2002, Phys. Rev. E, 65, 066203
Spergel, D. N. & Hernquist, L. 1992, ApJ, 397, L75
Spitzer, L. J. & Chevalier, R. A. 1973, ApJ, 183, 565
Stadel, J. G. 2001, Ph.D. Thesis
Taylor, J. E. & Navarro, J. F. 2001, ApJ, 563, 483
Terzić, B. & Kandrup, H. E. 2004, MNRAS, 347, 957
Valluri, M. 1993, ApJ, 408, 57
Valluri, M. & Merritt, D. 1998, ApJ, 506, 686
Valluri, M. & Merritt, D. 2000, in The Chaotic Universe, Proceedings of the Second ICRA Network Workshop, Advanced Series in Astrophysics and Cosmology, vol.10, Edited by V. G. Gurzadyan and R. Ruffini, World Scientific, 2000, p.229, ed. V. G. Gurzadyan & R. Ruffini, 229–+
Velazquez, H. & White, S. D. M. 1999, MNRAS, 304, 254
White, S. D. M. 1976, MNRAS, 174, 467
Zentner, A. R., Berlind, A. A., Bullock, J. S., Kravtsov, A. V., & Wechsler, R. H. 2005, ApJ, 624, 505
Zhao, H. 1996, MNRAS, 278, 488
Zwicky, F. 1939, Proc. Natl. Acad. Sci., 25, 604